A Dirac point insulator with topologically non-trivial surface states

D. Hsieh, D. Qian, L. Wray, Y. Xia, Y.S. Hor, R.J. Cava, and M.Z. Hasan

Topics:

1. Confirming the bulk nature of electronic bands by comparison with theoretical calculations
2. Spin-orbit coupling is responsible for the unique (Dirac) dispersion of the bulk bands near E_F
3. Matching the surface state Fermi crossings to the topology of the surface Fermi surface

1. Confirming the bulk nature of electronic bands by comparison with theoretical calculations

In an ARPES experiment (Fig.S1a), three dimensional (3D) dispersive bulk electronic states can be identified as those that disperse with incident photon energy, whereas surface states do not. As an additional check that we have indeed correctly identified the bulk bands of $Bi_{0.9}Sb_{0.1}$ in Figs 1 and 2, we also measured the dispersion of the deeper lying bands well below the Fermi level (E_F) and compared them to tight binding theoretical calculations of the bulk bands of pure bismuth following the model of Liu and Allen (1995)[22]. A tight-binding approach is known to be valid since $Bi_{0.9}Sb_{0.1}$ is not a strongly correlated electron system. As $Bi_{0.9}Sb_{0.1}$ is a random alloy (Sb does not form a superlattice[17]) with a relatively small Sb concentration (~0.2 Sb atoms per rhombohedral unit cell), the deeper lying band structure of $Bi_{0.9}Sb_{0.1}$ is expected to follow that of pure Bi because the deeper lying (localized wave function) bands of $Bi_{0.9}Sb_{0.1}$ are not greatly

affected by the substitutional disorder, and no additional back folded bands are expected to arise. Since these deeper lying bands are predicted to change dramatically with k_z, they help us to finely determine the experimentally probed k_z values. Fig.S2f shows the ARPES second derivative image (SDI) of a cut parallel to $\overline{K}\overline{M}\overline{K}$ that passes through the L point of the 3D Brillouin zone (BZ), and Fig.S2h shows a parallel cut that passes through the 0.3 $\overline{XL}$ point (Fig.S2c). The locations of these two cuts in the 3D bulk BZ were calculated from the kinematic relations described in the Methods section, from which we can construct the constant energy contours shown in Fig. S1c. By adjusting θ such that the in-plane momentum k_x is fixed at approximately 0.8 $Å^{-1}$ (the surface $\overline{M}$ point), at a photon energy $h\nu$=29 eV, electrons at the Fermi energy (E_B=0 eV) have a k_z that corresponds to the *L* point in the 3rd bulk BZ. By adjusting θ such that the in-plane momentum k_x is fixed at approximately -0.8 $Å^{-1}$, at a photon energy $h\nu$=20 eV, electrons at a binding energy of -2 eV have a k_z near 0.3 $\overline{XL}$.

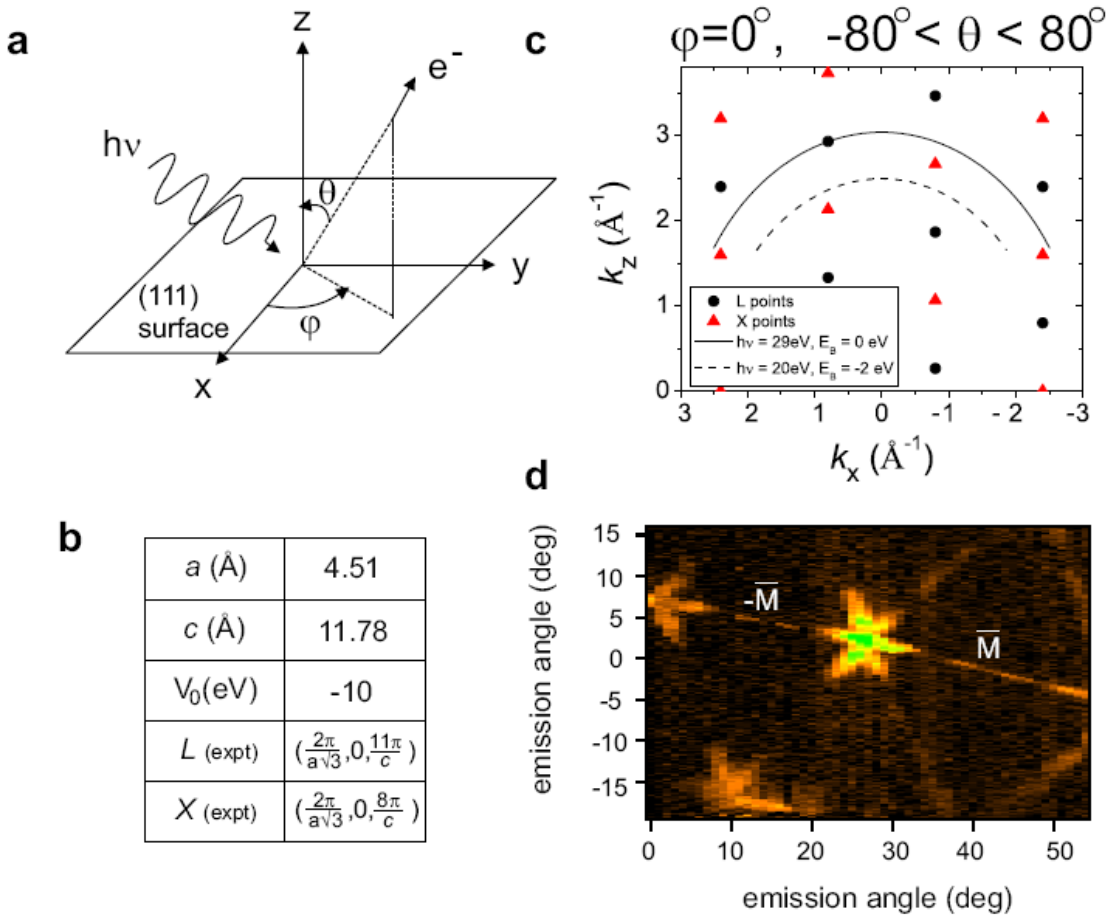

b

a (Å)	4.51
c (Å)	11.78
V_0(eV)	-10
L (expt)	$(\frac{2\pi}{a\sqrt{3}},0,\frac{11\pi}{c})$
X (expt)	$(\frac{2\pi}{a\sqrt{3}},0,\frac{8\pi}{c})$

Figure S1: Method of locating high symmetry bulk reciprocal lattice points of $Bi_{0.9}Sb_{0.1}$ using incident photon energy modulated ARPES. a, Geometry of an ARPES experiment. **b,** Key parameters relevant to the calculation of the positions of the high symmetry points in the 3D BZ. The lattice constants refer to the rhombohedral A7 lattice structure. **c,** Location of *L* and *X* points of the bulk BZ in the k_x - k_z plane together with the constant energy contours that can be accessed by changing the angle θ. **d,** Near E_F intensity map (hν = 55 eV) of the Fermi surface formed by the surface states covering an entire surface BZ, used to help locate various in-plane momenta, in units of the photoelectron emission angle along two orthogonal spatial directions. The electron pockets near $\bar{M}$ in Fig.2c (main text) appear as lines in Fig.S1d due to relaxed k-resolution in order to cover a large k-space in a single shot.

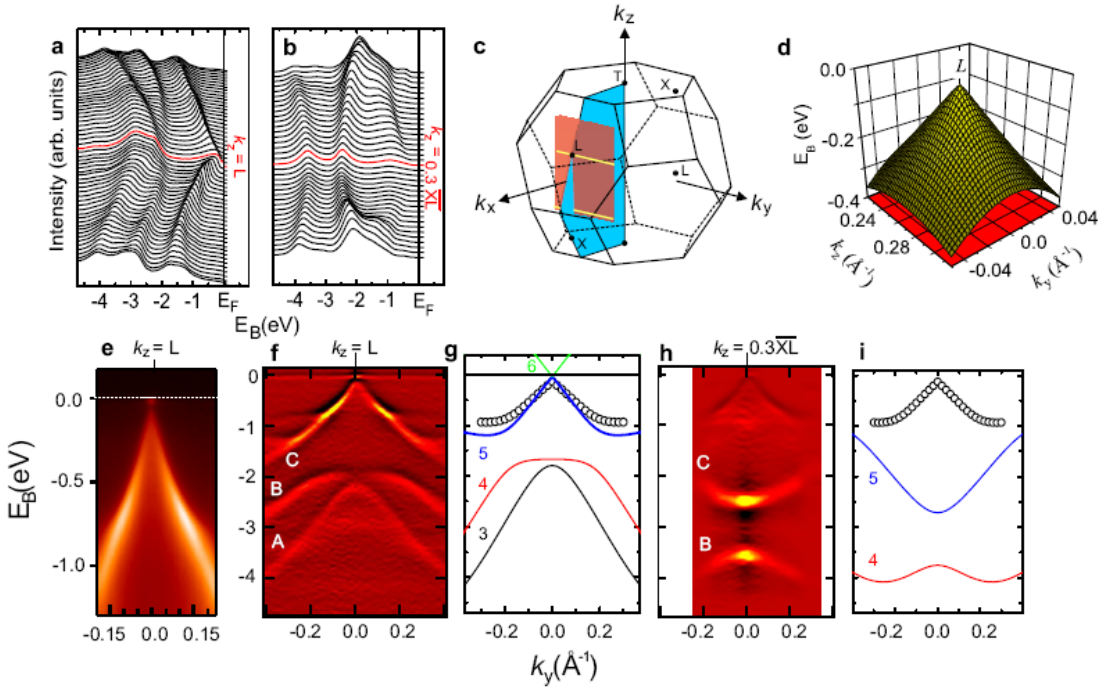

Figure S2: Identification of the bulk band features of $Bi_{0.9}Sb_{0.1}$. Experimental band-structure determined by ARPES is compared to bulk tight-binding calculations of bismuth to further identify the deeper lying bulk bands and their symmetry origins. a, Energy distribution curves (EDCs) along a k-space cut given by the upper yellow line shown in schematic **c** which goes through the bulk L point in the 3rd BZ (hν=29eV). The corresponding ARPES intensity in the vicinity of L is shown in **e**. **b,** EDCs along the lower yellow line of **c** which goes through the point a fraction 0.3 of the k-distance from X to L (hν=20eV), showing a dramatic change of the deeper lying band dispersions. (This cut was taken at a k_x value equal in magnitude but opposite in sign to that in **a** as described in the SI text). **f,h,** The ARPES second derivative images (SDI) of the raw data shown in **a** and **b** to reveal the band dispersions. The flat band of intensity at E_F is an artifact of taking SDI. **g,i,** Tight binding band calculations of bismuth including spin-orbit coupling, using Liu and Allen model[22], along the corresponding experimental cut directions shown in **f** and **h**. The bands (colored solid lines) labelled 3 to 6 are derived from

the symmetries associated with the *6p*-orbitals and their dispersion is thus strongly influenced by spin-orbit coupling. The inter-band gap between bands 5 and 6 is barely visible on the scale of Fig. S2**g**. The circled curves mark the surface state dispersion which is present at all measured photon energies (no k_z dispersion). There is a close match of the bulk band dispersion between the data and calculations, confirming the presence of strong spin-orbit coupling. **d,** Tight binding valence band (5) dispersion of bismuth in the k_y-k_z momentum plane showing linearity along both directions. The close match between data and calculation along k_y suggests that the dispersion near E_F along k_z is also linear.

There is a clear k_z dependence of the dispersion of measured bands A, B and C, pointing to their bulk nature. The bulk origin of bands A, B and C is confirmed by their good agreement with tight binding calculations (bands 3, 4 and 5 in Figs S2g and i), which include a strong spin-orbit coupling constant of 1.5 eV derived from bismuth[22]. Band 3 drops below -5eV at the 0.3 $\overline{XL}$ point. The slight differences between the experimentally measured band energies and the calculated band energies at $k_y = 0$ $Å^{-1}$ shown in Fig.S2f-i are due to the fact that the ARPES data were collected in a single shot, taken in constant θ mode. This means that electrons detected at different binding energies will have slightly different values of k_z as described in Methods, whereas the presented tight binding calculations show all bands at a single k_z. We checked that the magnitude of these band energy differences is indeed accounted for by this explanation. Even though the L_a and L_s bands in $Bi_{0.9}Sb_{0.1}$ are inverted relative to those of pure semimetallic Bi, calculations show that near E_F, apart from an insulating gap, they are “mirror” bands in terms of k dispersion (see bands 5 and 6 in Fig.S2g). Such a close match to calculations, which also predict a linear dispersion along the k_z cut near E_F (Fig.S2d), provides strong

support that the dispersion of band C, near E_F, is in fact linear along k_z. Focusing on the **Λ**-shaped valence band at L, the EDCs (Fig.S2a) show a single peak out to $k_y \approx \pm 0.15$ Å^{-1} demonstrating that it is composed of a single band feature. Outside this range however, an additional feature develops on the low binding energy side of the main peak in the EDCs, which shows up as two well separated bands in the SDI image (Fig.2f) and signals a splitting of the band into bulk representative and surface representative components (Fig.S2a,f). Unlike the main peak that disperses strongly with incident photon energy, this shoulder-like feature is present and retains the same **Λ**-shaped dispersion near this k-region (open circles in Figs S2g and i) for all photon energies used, supporting its 2D surface character. This behaviour is quite unlike bulk band C, which attains the **Λ**-shaped dispersion only near 29 eV (see main text Fig. 2b).

2. Spin-orbit coupling is responsible for the unique Dirac-like dispersion behaviour of the bulk bands near E_F :

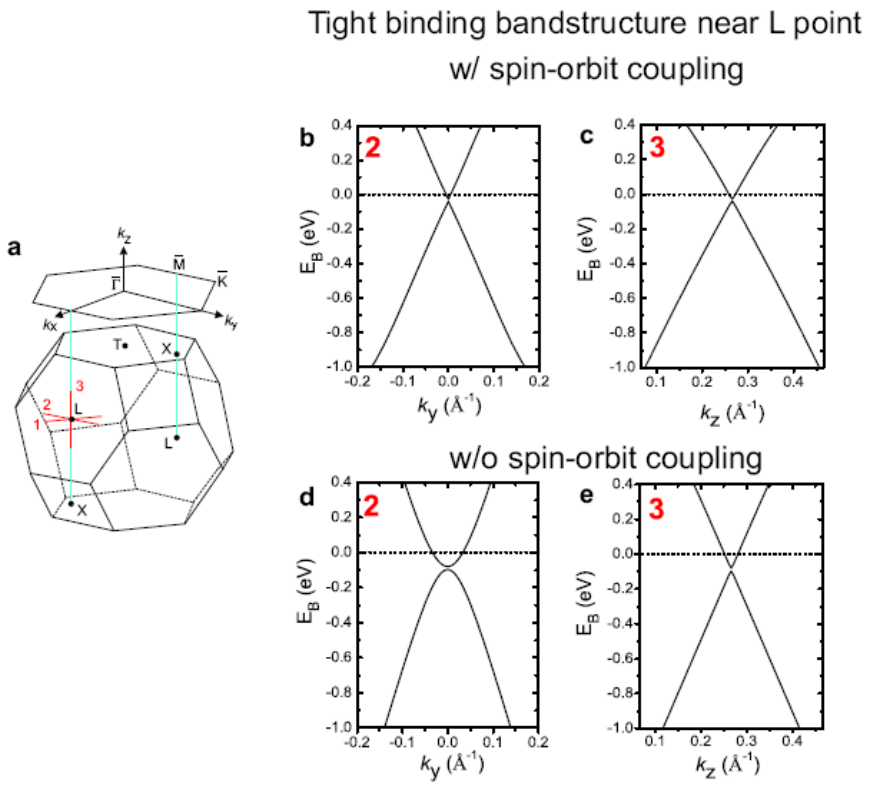

Figure S3: Spin-orbit coupling has a profound effect on the band structure of bismuth near L point. a, Schematic of the bulk 3D BZ and the projected BZ of the (111) surface. **b,c,** Calculated tight binding band structure of bismuth including a spin-orbit coupling strength of 1.5 eV[22] along two orthogonal cuts through the *L* point in the 1st bulk BZ. **d,e,** Tight binding band structure along the same two directions as **b** and **c** calculated without spin-orbit coupling. The inter-band gap of 13.7 meV is barely visible on the scale of **b** and **c**.

According to theoretical models, a strongly spin-orbit coupled bulk band structure is necessary for topological surface states to exist[7-11]. Therefore it is important to show that our experimentally measured bulk band structure of $Bi_{0.9}Sb_{0.1}$ can only be accounted for

by calculations that explicitly include a large spin-orbit coupling term. As shown in the previous section, the measured bulk band dispersion of $Bi_{0.9}Sb_{0.1}$ generally follows the calculated bulk bands of pure Bi from a tight binding model. The dispersion of the bulk valence and conduction bands of pure bismuth near E_F at the L point from such a tight binding calculation[22] with a spin-orbit coupling constant of 1.5eV are shown in Fig. S3b and c, which show a high degree of linearity. The high degree of linearity can be understood from a combination of the large Fermi velocity ($v_F \approx 6$ eV Å along k_y) and small inter-band (below E_F) gap $\Delta = 13.7$ meV (Fig. S3). This calculated inter-band gap of Bi (13.7 meV) is smaller than our measured lower limit of 50 meV (main text Fig. 1a) for the insulating gap of $Bi_{0.9}Sb_{0.1}$. To illustrate the importance of spin-orbit coupling in determining the band structure near L, we show the dispersion along k_y and k_z calculated without spin-orbit coupling (Fig. S3d and e). While the dispersion along k_z is not drastically altered by neglecting the spin-orbit coupling, the dispersion along k_y changes from being linear to highly parabolic. This is further evidence that our measured Dirac point can be accounted for only by including spin-orbit coupling. *A strong spin-orbit coupling constant acts as an internal quantizing magnetic field for the electron system*[6] *which can give rise to a quantum spin Hall effect without any externally applied magnetic field*[3,4,5,12,37]*. Therefore, the existence or the spontaneous emergence of the surface or boundary states does not require an external magnetic field.*

3. Matching the surface state Fermi crossings and the topology of the surface Fermi surface in bulk insulating $Bi_{0.9}Sb_{0.1}$

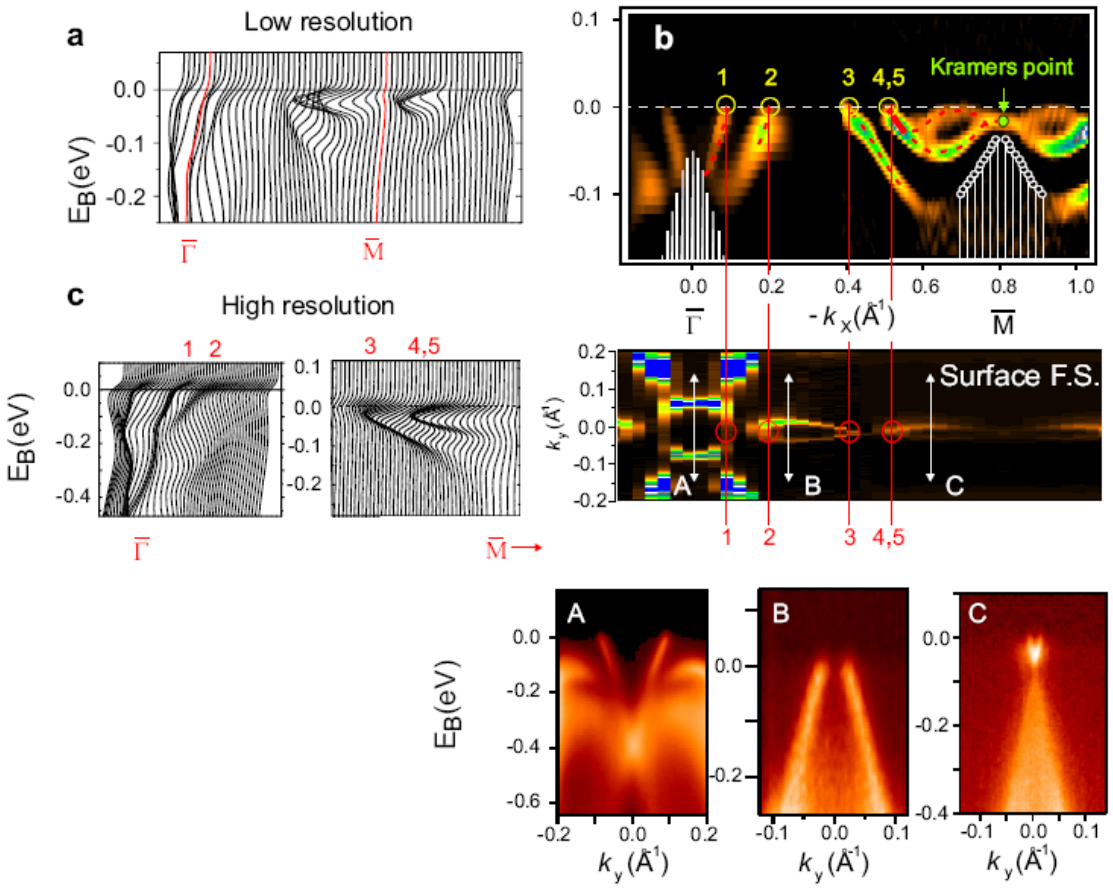

Figure S4: The Kramers' point, the gapless nature and topology of surface states in insulating $Bi_{0.9}Sb_{0.1}$ is revealed through high spatial and k-resolution ARPES. a, Energy distribution curves (EDCs) of a low resolution ARPES scan along the surface $\overline{\Gamma}$ - $\overline{M}$ cut of $Bi_{0.9}Sb_{0.1}$. **b,** The surface band dispersion second derivative image along $\overline{\Gamma}$ - $\overline{M}$ obtained by piecing together four high resolution ARPES scans. See main text Fig.3 for explanation of other features. **c,** EDCs of high resolution ARPES scans in the vicinity of surface Fermi crossings 1 and 2 and crossings 3, 4 and 5 (left panels). These crossings form the surface Fermi surface shown in

the upper right panel of **c** (see also main text Fig.2). High resolution ARPES scans along cut directions A, B and C are further evidence for a surface Fermi surface.

In order to count the number of singly degenerate surface state Fermi crossings[24,28,38] along the $\overline{\Gamma}$ - $\overline{M}$ cut of the surface BZ, high photon energy ARPES scans, which allow mapping of the entire k range from $\overline{\Gamma}$ - $\overline{M}$ to fall within the detector window at the expense of lower instrument resolution, were taken to preliminarily identify the k-space locations of the Fermi crossings (Fig. S4a). Having determined where these surface state Fermi crossings lie in k-space, we performed several high resolution ARPES scans, each covering a successive small k interval in the detector window, in order to construct a high resolution band mapping of the surface states from $\overline{\Gamma}$ to $\overline{M}$. The second derivative image of the surface band dispersion shown in Fig.S4b was constructed by piecing together four such high resolution scans. Fig.S4c shows energy distribution curves of high resolution ARPES scans in the vicinity of each surface Fermi crossing, which together give rise to the surface Fermi surface shown. No previous work[24,26-30,35,36] has reported the band dispersion near the L-point (thus missing the Dirac bands) or resolved the Kramers point near the $\overline{M}$ point, which is crucial to determine the topology of the surface states. For this reason there is no basis for one-to-one comparison with previous work, since no previous ARPES data exists in the analogous k-range. Note that surface band dispersions along the cuts A, B and C are highly linear. This is indirect evidence for the existence of the bulk Dirac point since surface states are formed when the bulk state wave functions are subjected to the boundary conditions at the cleaved plane.

37. Sheng, L., Sheng, D. N., Ting, C. S. & Haldane, F. D. M. Nondissipative spin Hall effect via quantized edge transport. *Phys. Rev. Lett.* **95**, 136602 (2005).

38. Kim, T. K. *et al.* Evidence against a charge density wave on Bi(111). *Phys. Rev.* **B 72**, 085440 (2005).